AGU PUBLICATIONS

Paleoceanography

RESEARCH ARTICLE
10.1002/2015PA002822

Key Points:
- Benthic foraminiferal $\delta^{13}C$ and $\delta^{18}O$ preserved despite recrystallization of tests
- Orbital cycles preserved in isotope record indicate recrystallization in < 100 kyr
- Transfer of U1336 magnetostratigraphy to Sites U1337 and U1338 possible

Supporting Information:
- Texts S1 and S2, Figures S1–S8, and Tables S1–S3

Correspondence to:
J. Voigt,
jvoigt@marum.de

Citation:
Voigt, J., E. C. Hathorne, M. Frank, and A. Holbourn (2016), Minimal influence of recrystallization on middle Miocene benthic foraminiferal stable isotope stratigraphy in the eastern equatorial Pacific, *Paleoceanography*, *31*, 98–114, doi:10.1002/2015PA002822.

Received 25 APR 2015
Accepted 15 DEC 2015
Accepted article online 18 DEC 2015
Published online 16 JAN 2016

Minimal influence of recrystallization on middle Miocene benthic foraminiferal stable isotope stratigraphy in the eastern equatorial Pacific

Janett Voigt[1,2], Ed C. Hathorne[1], Martin Frank[1], and Ann Holbourn[3]

[1]GEOMAR Helmholtz Centre for Ocean Research Kiel, Kiel, Germany, [2]Now at MARUM - Center for Marine Environmental Sciences, Bremen, Germany, [3]Institute of Geosciences, Christian-Albrecht-University, Kiel, Germany

Abstract Stable carbon and oxygen isotopes ($\delta^{13}C$ and $\delta^{18}O$) of foraminiferal tests are amongst the most important tools in paleoceanography, but the extent to which recrystallization can alter the isotopic composition of the tests is not well known. Here we compare three middle Miocene (16–13 Ma) benthic foraminiferal stable isotope records from eastern equatorial Pacific sites with different diagenetic histories to investigate the effect of recrystallization. To test an extreme case, we analyzed stable isotope compositions of benthic foraminifera from Integrated Ocean Drilling Program Site U1336, for which the geochemistry of bulk carbonates and associated pore waters indicates continued diagenetic alteration in sediments > 14.7 Ma. Despite this diagenetic overprinting, the amplitudes and absolute values of the analyzed U1336 stable isotopes agree well with high-resolution records from better preserved Sites U1337 and U1338 nearby. Our results suggest that although benthic foraminiferal tests of all three sites show some degree of textural changes due to recrystallization, they have retained their original stable isotope signatures. The good agreement of the benthic foraminiferal stable isotope records demonstrates that recrystallization occurred extremely rapidly (< 100 kyr) after deposition. This is confirmed by the preservation of orbital cyclicities in U1336 stable isotope data and $\delta^{18}O$ values being different to inorganic calcite that would precipitate from U1336 pore waters during late recrystallization. The close similarity of the benthic foraminiferal stable isotope records between the sites allows the well-resolved paleomagnetic results of Site U1336 to be transferred to Sites U1337 and U1338 improving the global geological timescale.

1. Introduction

The calcite tests of foraminifera preserved in marine sediments are widely used to reconstruct a range of marine environmental parameters including past seawater temperature, salinity, and global ice volume [e.g., *Lear et al.*, 2000; *Zachos et al.*, 2001b, 2008]. However, ancient foraminiferal tests are often altered after deposition by recrystallization on the seafloor and in the sediment, during which the original biogenic calcite is partially dissolved and subsequently replaced by secondary (inorganic) calcite. Significant changes in stable isotope ($\delta^{13}C$ and $\delta^{18}O$) and Mg/Ca ratios of recrystallized planktonic foraminifera have been reported, which can bias paleotemperatures and interpretations of paleoclimatic variability [*Pearson et al.*, 2001; *Regenberg et al.*, 2007; *Sexton et al.*, 2006]. *Pearson et al.* [2001] found that diagenetic effects on planktonic $\delta^{18}O$ could explain the "cool tropic paradox" of the Paleocene and Eocene given that altered planktonic foraminifera tend to have higher $\delta^{18}O$ values, indicating cooler temperatures than unaltered contemporaneous tests. These authors also found that well-preserved foraminifera from clay-rich sediments appear "glassy" under the light microscope when wet. In contrast, less well preserved tests are opaque ("frosty") under the light microscope [*Pearson and Burgess*, 2008; *Sexton et al.*, 2006]. Scanning electron microscope (SEM) imaging revealed that the wall structure of well-preserved foraminiferal tests consists of fine, distinct calcite crystals, whereas in less well preserved foraminifera the original submicron-sized calcite crystals have been replaced by micron-sized secondary calcite crystals [*Hodell et al.*, 2007; *Pearson and Burgess*, 2008; *Sexton and Wilson*, 2009; *Sexton et al.*, 2006]. Besides this change in crystal structure, recrystallization is often accompanied by overgrowth with secondary calcite on the inner and outer surface of the tests in the form of coarser crystals and infilling of the tests with detrital material and coccoliths [*Hodell et al.*, 2007; *Pearson and Burgess*, 2008; *Regenberg et al.*, 2007; *Sexton and Wilson*, 2009; *Sexton et al.*, 2006]. Furthermore, heavily recrystallized tests become physically weaker and therefore break more easily, thereby leading to increasing fragmentation [e.g., *Pearson et al.*, 2015]. The "glassy" tests of planktonic and benthic foraminifera in clay-rich sediments are

considered to retain the most reliable geochemical signatures because of their excellent preservation [e.g., *Bown et al.*, 2008; *Pearson and Burgess*, 2008; *Pearson et al.*, 2001, 2007; *Sexton and Wilson*, 2009; *Sexton et al.*, 2006; *Stewart et al.*, 2004], whereas most carbonate-rich pelagic oozes containing foraminiferal tests are prone to recrystallization [e.g., *Sexton et al.*, 2006; *Pearson and Burgess*, 2008; *Sexton and Wilson*, 2009]. Additionally, very low sedimentation rates and high geothermal gradients have been suggested to significantly influence the $\delta^{18}O$ of benthic foraminiferal tests [e.g., *Edgar et al.*, 2013; *Sexton and Wilson*, 2009]. However, a recent study indicated that the stable isotope compositions of benthic foraminifera from Oligocene age nannofossil oozes from the eastern equatorial Pacific show negligible intersite offsets, although the investigated sites had different recrystallization histories and the preservation of foraminiferal tests differed markedly [*Edgar et al.*, 2013]. Two high-resolution middle Miocene benthic foraminiferal stable isotope records from Integrated Ocean Drilling Program (IODP) Sites U1337 and U1338 also show good agreement [*Holbourn et al.*, 2014; *Tian et al.*, 2013]. Both sites have comparable sedimentation rates, geothermal gradients, and carbonate contents [*Pälike et al.*, 2010] suggesting comparable recrystallization histories during the middle Miocene. Shipboard investigations indicated good preservation of the benthic foraminifera of Sites U1337 and U1338 during the investigated time interval [*Pälike et al.*, 2010]. Further studies focusing on Site U1338 confirmed that late Miocene and Pliocene benthic foraminifera [*Drury et al.*, 2014] and middle Miocene planktonic foraminifera are well preserved at this site [*Fox and Wade*, 2013], although the appearance of planktonic foraminiferal tests under the light microscope varied between glassy and frosty (B. Wade, personal communication, 2015).

Previous studies about diagenetic effects on the geochemistry of foraminiferal tests have focused on specific time intervals [e.g., *Kozdon et al.*, 2013; *Pearson et al.*, 2001; *Sexton et al.*, 2006; *Sexton and Wilson*, 2009]; however, extended, high-resolution (better than 20 kyr) time series that allow the assessment of how well recrystallized tests record climatic variations are still lacking.

To test the reliability of benthic foraminiferal stable isotope records, we examined the pronounced Miocene variations recorded in eastern equatorial Pacific sediments of selected Sites U1336, U1337, and U1338, which were subjected to variable carbonate preservation. The three sites compared had similar initial sediment compositions but different burial histories [*Pälike et al.*, 2010]. Additionally, the cores of IODP Expeditions 320/321 recovered one of the most complete Miocene sections allowing detailed studies at the paleoequator in the Pacific. The Cenozoic long-term cooling trend from the warm greenhouse climate of the Paleogene to the Neogene icehouse climate [e.g., *Zachos et al.*, 2001a] was interrupted by an extended warm interval from ~17 to 14.7 Ma, termed the Middle Miocene Climate Optimum [e.g., *Flower and Kennett*, 1993; *Holbourn et al.*, 2005, 2007]. This interval is characterized by 100 kyr eccentricity variability and shows low mean $\delta^{18}O$ values but a high variability in both $\delta^{13}C$ and $\delta^{18}O$ [*Holbourn et al.*, 2007, 2014]. Characteristic for the middle Miocene is the distinct maxima in $\delta^{13}C$ of the "Monterey Carbon Isotopic Excursion" [e.g., *Holbourn et al.*, 2007; *Vincent and Berger*, 1985], which was associated with 400 kyr long eccentricity cycles [e.g., *Holbourn et al.*, 2005, 2007, 2014; *Shevenell et al.*, 2004; *Woodruff and Savin*, 1991]. During the Monterey Excursion, $\delta^{13}C$ and $\delta^{18}O$ covaried indicating a close coupling of the global carbon cycle and climate system [e.g., *Flower and Kennett*, 1993; *Vincent and Berger*, 1985; *Woodruff and Savin*, 1991]. It was suggested that periodic increases in organic carbon burial caused the $\delta^{13}C$ maxima and thereby reduced atmospheric CO_2, resulting in global cooling [*Flower and Kennett*, 1993, 1994; *Vincent and Berger*, 1985; *Woodruff and Savin*, 1991]. This cooling trend culminated in a major cooling event, associated with massive ice-sheet expansion on Antarctica at ~13.9 Ma [e.g., *Flower and Kennett*, 1994; *Holbourn et al.*, 2005, 2007]. However, to date only a few high-resolution foraminiferal stable isotope records cover this important interval [*Holbourn et al.*, 2005, 2007, 2014; *Shevenell et al.*, 2004, 2008; *Tian et al.*, 2013, 2014].

One overall aim of IODP Expeditions 320/321 was to validate and extend the astronomical calibration of the geological timescale for the Cenozoic by using biostratigraphy, chemostratigraphy, and magnetostratigraphy at the equator [*Pälike et al.*, 2010]. For Sites U1337 and U1338, high-resolution benthic foraminiferal stable isotope based chronologies exists [*Holbourn et al.*, 2014; *Tian et al.*, 2013], but the polarity chronologies for this time interval are poorly constrained [*Pälike et al.*, 2010]. On the other hand, at Site U1336, a well-resolved magnetic data set was established, in particular for the early to middle Miocene [*Ohneiser et al.*, 2013]. It would therefore be useful to transfer the paleomagnetic results of Site U1336 to Sites U1337 and U1338 through correlation of the U1336 benthic foraminiferal stable isotope record from this study, to improve the global geological timescale.

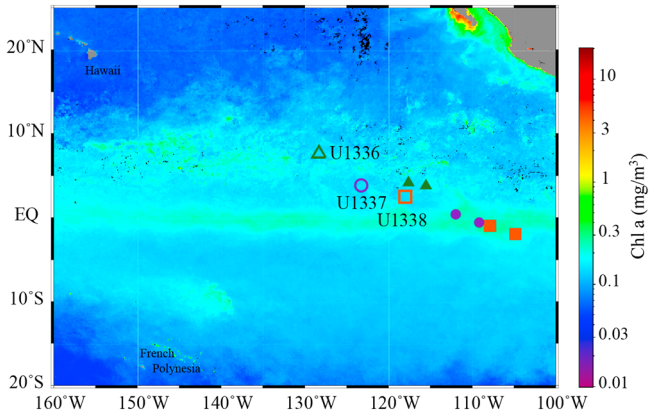

Figure 1. Equatorial Pacific map showing the averaged chlorophyll *a* data from June 2012 to 2014 [*Feldmann*, 2014] representative of modern primary productivity of the study area. The present location of the PEAT sites included in this study is indicated by larger, open symbols. Their backtracked positions from 16 and 13 Ma, given as closed symbols, were estimated from *Pälike et al.* [2010]; the oceanic crust below the sites originated from the East Pacific Rise and moved in a north-west direction.

Here we present benthic foraminiferal stable isotope data from IODP Site U1336, which were generated to precisely constrain specific intervals within the middle Miocene for further study. The U1336 benthic stable isotope record is compared with high-resolution records from nearby Sites U1337 [*Tian et al.*, 2013] and U1338 [*Holbourn et al.*, 2014] to evaluate possible offsets caused by recrystallization on the geochemistry of foraminiferal tests. Analyses of bulk carbonate Sr parameters from the three sites indicated different recrystallization histories, although Sites U1337 and U1338 are similar for the time interval investigated here [*Voigt et al.*, 2015]. During recrystallization of biogenic carbonates, Sr is released from the carbonates to the pore waters making pore water Sr concentrations diagnostic for recrystallization [e.g., *Baker et al.*, 1982; *Elderfield and Gieskes*, 1982; *Gieskes et al.*, 1986; *Richter*, 1993; *Stout*, 1985]. As less Sr is incorporated into secondary calcite, diagenetically altered bulk carbonates exhibit generally lower Sr/Ca ratios [e.g., *Baker et al.*, 1982; *Delaney*, 1989]. Site U1336, in contrast to the other sites, has extensively altered bulk carbonates and active recrystallization is suggested for sections older than 20.2 Ma, as a consequence of an inferred large thermal gradient [*Voigt et al.*, 2015]. However, pore water $^{87}Sr/^{86}Sr$ ratios lower than contemporaneous seawater (Figure S1 in the supporting information) and generally lower bulk carbonate Sr/Ca ratios confirm more extensive recrystallization compared to the other sites in the section older than 14.7 Ma [*Voigt et al.*, 2015]. Here we show that even in carbonate sediments with such clear geochemical signs of persistent recrystallization the stable isotope composition of benthic foraminifera is not altered.

2. Materials and Methods

2.1. Site Description

Sites U1336, U1337, and U1338 were recovered during the IODP Pacific Equatorial Age Transect (PEAT) Expeditions 320/321 (Figure 1), and detailed lithological descriptions are provided in *Pälike et al.* [2010]. All depths are given in revised meters composite depth (rmcd) [*Wilkens et al.*, 2013]. Site U1336 is located in the eastern equatorial Pacific (7°42.067′N, 128°15.253′W) close to the Clipperton Fracture Zone (~30 km) in a water depth of 4286 m [*Pälike et al.*, 2010]. The site was shallower during the middle Miocene at 3800–3900 m [*Pälike et al.*, 2012]. Carbonate sediments nannofossil ooze (on average 87.3% $CaCO_3$) [*Pälike et al.*, 2010] accumulated through the early Oligocene to middle Miocene at Site U1336 until the site subsided below the carbonate compensation depth at around 12 Ma resulting in ~2.8 m of clay accumulation thereafter [*Pälike et al.*, 2010, 2012].

Site U1337 (3°50.007′N, 123°12.356′W) is located 700 km southeast of Site U1336 in a water depth of 4461 m and a reconstructed middle Miocene water depth of 3800–4050 m [*Pälike et al.*, 2012]. Site U1338 (2°30.469′N, 117°58.178′W) is located 1300 km southeast of Site U1336 in a water depth of 4200 m [*Pälike et al.*, 2010] corresponding to a middle Miocene water depth of 3200–3600 m [*Pälike et al.*, 2012]. The Miocene successions of Sites U1337 and U1338 consist of carbonate-rich nannofossil and microfossil oozes containing on average 61.7% and 71.2% $CaCO_3$, respectively [*Pälike et al.*, 2010]. As the Pacific plate moved away from the East Pacific Rise, the sites left the equatorial zone of high productivity between 2° north and south of the equator during different time intervals (Figure 1). Sites U1337 and U1338 remained in the high-productivity area with a deep carbonate compensation depth for longer periods of time, resulting in higher sedimentation rates compared to Site U1336 [*Pälike et al.*, 2010] and thus presumably in better carbonate preservation.

2.2. Sample Preparation for $\delta^{13}C$ and $\delta^{18}O$ Measurements

Samples from Site U1336 were taken from 12.04 to 48.19 rmcd at 6 to 15 cm intervals (corresponding to a 5.1 to 17.8 kyr temporal resolution). The sampling was increased from 2 to 6 cm (~1.7–5.1 kyr) in the section between 37.23 and 41.94 rmcd corresponding to 15.1–15.5 Ma. Samples of 20 cm^3 volume were freeze-dried and then washed over a 63 μm sieve, and the residue was dried at 40°C and sieved into different size fractions. Specimens of the epifaunal benthic foraminiferal species *Cibicidoides wuellerstorfi* and *Cibicidoides mundulus* were picked from the > 250 μm fraction for stable carbon and oxygen isotope analyses, the same species and size fraction used by *Holbourn et al.* [2014] for Site U1338. In contrast, *Tian et al.* [2013] analyzed *Cibicidoides* spp. from the > 150 μm fraction at Site U1337. Analyses of mixed *C. wuellerstorfi* and *C. mundulus* were performed for about half of the samples in Site U1336; monospecific tests were measured for the remaining samples. In the interval between 43.20 and 48.19 rmcd, only *C. mundulus* was analyzed, given that *C. wuellerstorfi* was not present in this section. For 20 samples, these species were also picked from the 150–250 μm fraction. For 26 samples where foraminifera were scarce, only 1 or 2 individuals were analyzed. Generally, between three and six individual tests per sample were cracked into large fragments, cleaned in ethanol in an ultrasonic bath, and dried at room temperature following the method described in *Holbourn et al.* [2005].

2.3. $\delta^{13}C$ and $\delta^{18}O$ Analyses

Isotope measurements were performed on a Thermo MAT 253 mass spectrometer at GEOMAR equipped with a Carbo-Kiel device Type IV. Samples were reacted with 99% H_3PO_4 at 74°C. The $\delta^{13}C$ and $\delta^{18}O$ data are given relative to the Vienna Peedee belemnite (VPDB) and are referenced to the National Institute of Standards and Technology carbonate isotope standard NBS 19. The measured values were not corrected for any vital effects to facilitate direct comparison with the records of Sites U1337 and U1338 [*Holbourn et al.*, 2014; *Tian et al.*, 2013]. The 1σ external reproducibility of the in-house carbonate standard (Solnhofen limestone) was ±0.06‰ and ±0.09‰ for $\delta^{13}C$ and $\delta^{18}O$, respectively ($n = 124$). Replicate measurements performed for 17% of the samples gave a mean reproducibility of ±0.09‰ and ±0.12‰ for $\delta^{13}C$ and $\delta^{18}O$, respectively. A *t* test ($p < 0.05$) was performed on monospecific results of 7% of the samples and indicated no significant offset of the $\delta^{13}C$ and $\delta^{18}O$ signatures between the two species as also reported by *Holbourn et al.* [2005, 2007, 2013, 2014]. The data for both species show a 1:1 relationship (Figure S2). Figure S2 might suggest interspecies offsets occur at higher $\delta^{13}C$ values, but the $\delta^{13}C$ values are possibly biased toward higher values by the relatively small amount of monospecific samples analyzed. Data sets are archived at the Data Publisher for Earth and Environmental Science (http://doi.pangaea.de/10.1594/PANGAEA.854835).

2.4. Orbital Tuning of Color Reflectance b*

We generated an orbitally tuned age model for Site U1336 by correlating the high-resolution color reflectance b* data of Site U1336 (2–5 cm) [*Pälike et al.*, 2010; *Wilkens et al.*, 2013] to calculated variations in eccentricity from *Laskar et al.* [2004] (Figure S3a) using AnalySeries Version 2.0 [*Paillard et al.*, 1996]. The temporal resolution of the U1336 isotope data is too low for independent tuning to an orbital solution, whereas the high-resolution reflectance parameter b* (blue-yellow), representing changes in lithology [e.g., *Blum*, 1997], exhibits well-defined cyclic variations. Color reflectance b* maxima, reflecting dark sediment layers corresponding to elevated proportions of radiolarians [*Pälike et al.*, 2010], were tuned to maxima (100 kyr) in eccentricity [*Laskar et al.*, 2004] because eccentricity maxima may have driven enhanced carbonate dissolution intensified by poorly ventilated bottom waters [*Holbourn et al.*, 2013, 2014, 2015]. Several studies showed that at eccentricity maxima, when the summer insolation and temperature were high, weathering and nutrient supply to the oceans increased, which led to increased export of terrestrial ^{13}C depleted organic carbon to the ocean or a change in the burial ratio of carbonate to organic carbon [e.g., *Pälike et al.*, 2006; *Zachos et al.*, 2008, 2010; *Ma et al.*, 2011; *Kirtland Turner*, 2014]. This organic carbon may have been remineralized efficiently resulting in increased carbonate dissolution [e.g., *Flower and Kennett*, 1994; *Holbourn et al.*, 2007, 2014; *Zachos et al.*, 2008, 2010; *Kirtland Turner*, 2014] and thus leaving mainly the siliceous fraction in the darker colored sediment bands. Age/depth tie points are presented in Table S1. However, the tuning of color reflectance b* appears less reliable for the intervals 15.75–15.25 Ma and 13.70–13.50 Ma, where the 100 kyr filtered record does not match the amplitudes of the target solution [*Laskar et al.*, 2004] (Figure S3b). For the interval from 14.6 to 14.1 Ma, where both filtered records do not show clear 100 kyr cyclicity, obliquity cycles prevail as

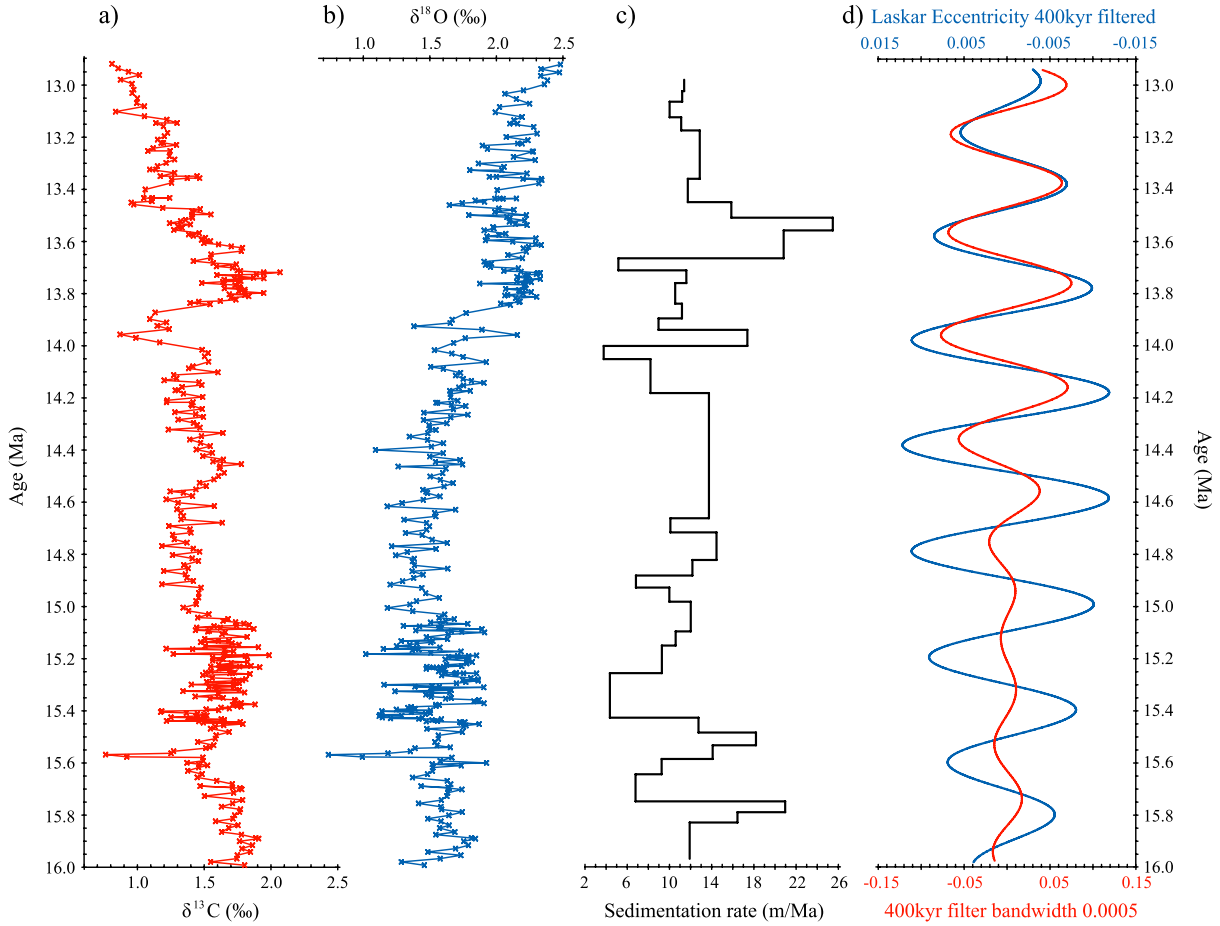

Figure 2. Comparison of Site U1336 (a) benthic $\delta^{13}C$, (b) benthic $\delta^{18}O$, (c) calculated sedimentation rates derived from the color reflectance b* age model, and (d) 400 kyr filtered eccentricity of *Laskar et al.* [2004] (blue) together with the benthic $\delta^{18}O$ record filtered for 400 kyr cycles (red) from 16.0 to 12.9 Ma.

clearly evident in the filtered color reflectance b* record (Figures S3b and S4). Nevertheless, the entire record was tuned to the 100 kyr eccentricity of *Laskar et al.* [2004] for simplicity.

3. Results

3.1. Benthic Foraminiferal $\delta^{18}O$ and $\delta^{13}C$ of Site U1336

The investigated interval of Site U1336 covers the time interval from 16.0 to 12.9 Ma (Figure 2) and includes a short interval (15.5–15.1 Ma) with a higher temporal resolution, comprising a section of darker colored sediment with a higher proportion of radiolarians [*Pälike et al.*, 2010].

The $\delta^{18}O$ and $\delta^{13}C$ data show synchronous changes from 16.0 to about 14.2 Ma. During this interval, the $\delta^{13}C$ values oscillate between 1.3 and 2.0‰ at amplitudes between 0.3 and 0.6‰, except for an abrupt decrease to 0.77‰ centered at 15.6 Ma (Figure 2a). Between 14.0 and 13.9 Ma, the $\delta^{13}C$ values decreased to 1.2–0.9‰, increased again until ~13.7 Ma reaching 2.1‰ and then decreased continuously thereafter. During 16.0–14.2 Ma, the $\delta^{18}O$ values fluctuated around a mean of 1.54‰ at amplitudes between 0.4 and 0.6‰ (Figure 2b). There was an abrupt negative shift reaching 0.74‰ at 15.6 Ma comparable to the $\delta^{13}C$ data (Figure 2b). After 14.2 Ma, $\delta^{18}O$ displays a trend to heavier values with the most rapid increase at ~13.9–13.8 Ma and then varied around a mean $\delta^{18}O$ of 2.11‰ between 13.8 and 12.9 Ma. Near 13.7 Ma the $\delta^{18}O$ record diverged from that of $\delta^{13}C$ in that the $\delta^{13}C$ values decreased continuously from ~13.7 to 12.9 Ma, whereas the $\delta^{18}O$ signatures remained stable (Figures 2a and 2b).

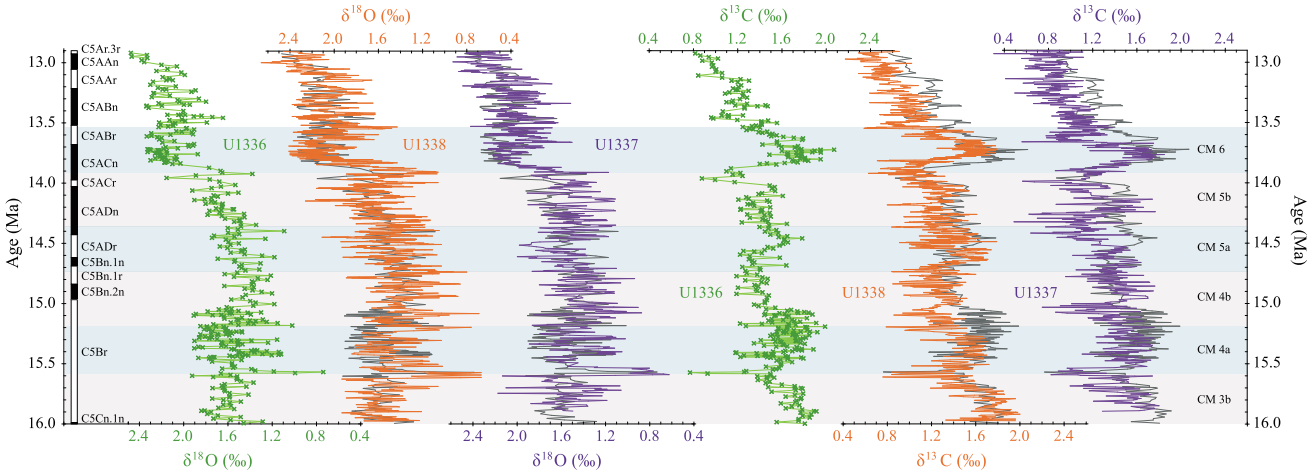

Figure 3. Comparison of benthic stable isotope time series of Site U1336 in green with U1337 in purple [*Tian et al.*, 2013] and U1338 in orange [*Holbourn et al.*, 2014]. Grey lines show the stable isotope record of Site U1336 overlapping with the ones of Sites U1337 and U1338 for direct comparison. The age of each stable isotope record is based on a different tuning approach, following the published age models for Sites U1337 [*Tian et al.*, 2013] and U1338 [*Holbourn et al.*, 2014]. Colored bands illustrate the carbon isotope maximum events (CM) of the Monterey Excursion (subdivisions by *Holbourn et al.* [2007]). The polarity stratigraphy of Site U1336 [*Ohneiser et al.*, 2013; *Pälike et al.*, 2010], based on the color reflectance b* age model (see also Table S3), is provided for comparison.

The Monterey Excursion [*Vincent and Berger*, 1985; *Woodruff and Savin*, 1991] can clearly be identified including the 400 kyr carbon isotope maxima (CM) events (CM 3b, CM 4a, CM 4b, CM 5a, CM 5b, and CM 6) according to the subdivisions of *Holbourn et al.* [2007] (Figure 3).

3.2. Astronomical Cycles in $\delta^{18}O$, $\delta^{13}C$, and Physical Property Data of Site U1336

The stable isotope data of Site U1336 show low-frequency variations that follow the long eccentricity cycles (400 kyr) (Figure 2), which is also evident from the recognition of the 400 kyr cycles of the Monterey Excursion (Figure 3). Comparison of the 400 kyr filtered $\delta^{18}O$ record with long eccentricity cycles from *Laskar et al.* [2004] documents a good match from ~14.7 to 12.9 Ma (Figure 2d). Prior to 14.7 Ma, the isotope record of Site U1336 does not match the target solution of *Laskar et al.* [2004] and lag behind by ~60 kyr possibly caused by the resolution of the data. During this interval (~16.0 to 14.6 Ma), short eccentricity cycles (100 kyr) are visible (Figure 4). Although the 100 kyr cycles are not very well defined, probably due to the sampling resolution, they match the filtered eccentricity [*Laskar et al.*, 2004] between 15.5 and 14.7 Ma (Figure 4b). Prior to that interval, the $\delta^{18}O$ record lags behind by ~30–50 kyr and is almost exactly out of phase (Figure 4b) most likely caused by the tuning method applied.

The astronomical cyclicities of sediment parameters, including color reflectance b*, magnetic susceptibility, and Gamma Ray Attenuation (GRA) bulk density, were also examined. The high-resolution color reflectance b* record (2–4 kyr) [*Pälike et al.*, 2010; *Wilkens et al.*, 2013] matches the 400 kyr cycles at 16.0–15.2 Ma and 13.9–12.9 Ma and, as described above (see section 2.4), shows good agreement with the 100 kyr cycles (Figure S4). The high-resolution record of magnetic susceptibility (2–3 kyr) [*Pälike et al.*, 2010; *Wilkens et al.*, 2013] matches well with the 400 kyr cycles between ~14.5 and 13.4 Ma and the 100 kyr cycles at 16.0–15.5 Ma, ~14.1–13.8 Ma, and ~13.5–12.9 Ma (Figure S5). The high-resolution record of GRA bulk density (2–3 kyr) [*Pälike et al.*, 2010; *Wilkens et al.*, 2013] matches the long eccentricity cycles between ~14.4 and 13.6 Ma, and the record agrees with the short eccentricity cycles at 16.0–15.2 Ma, at 14.9–14.7 Ma, and at ~13.5–12.9 Ma (Figure S6).

Low $\delta^{18}O$ values are associated with darker colored sediment bands (between 46.8 and 31.8 rmcd, corresponding to 15.9–14.6 Ma) (Figure 5), containing more radiolarians and clay [*Pälike et al.*, 2010], and are related to short warm intervals, when there was minimum ice volume and poor ventilation of the deep eastern Pacific during the Middle Miocene Climate Optimum [*Holbourn et al.*, 2007, 2014; *Lear et al.*, 2000; *Shevenell et al.*, 2008; *Zachos et al.*, 2001b]. Furthermore, the sediment parameters magnetic susceptibility and Gamma Ray Attenuation (GRA) bulk density are correlated with the darker colored sediment bands (Figure 5, see supporting information Text S1). These darker bands are related to carbonate dissolution events during warm intervals (see supporting information Text S1 for further explanations).

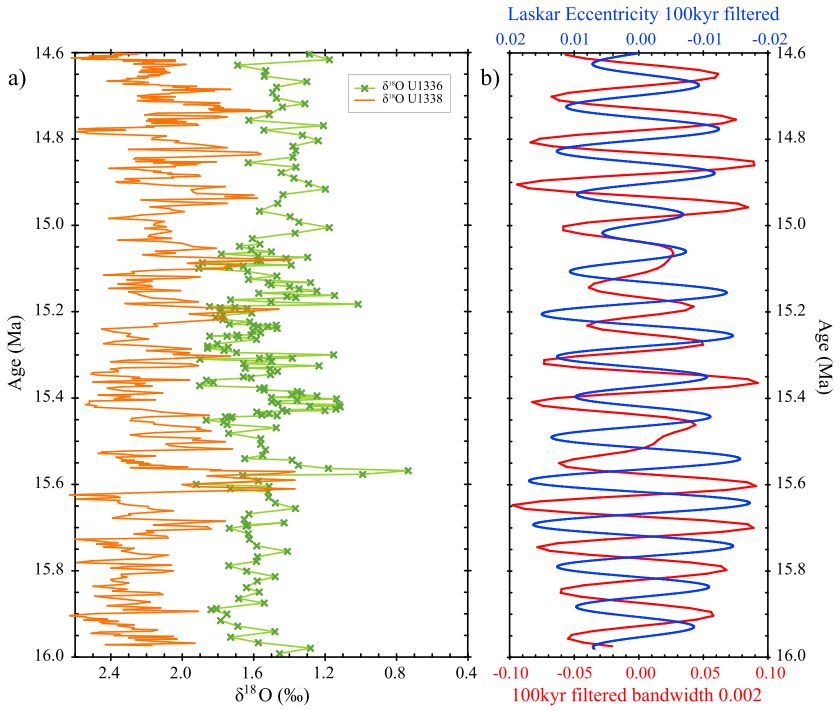

Figure 4. (a) $\delta^{18}O$ data of Site U1336 (green) shown for 16.0–14.6 Ma, including the time interval with highest resolution (1.7–5.1 kyr temporal resolution). The record is compared with that of Site U1338 (orange) [*Holbourn et al.*, 2014]. The $\delta^{18}O$ data of U1336 clearly indicate short eccentricity cycles (100 kyr) in agreement with the record of Site U1338. The record of U1338 was offset by +0.7‰ to facilitate comparison. (b) The 100 kyr filtered $\delta^{18}O$ record of Site U1336 (red) is compared to the 100 kyr filtered eccentricity of *Laskar et al.* [2004] (blue).

3.3. Comparison of the Benthic Foraminiferal $\delta^{18}O$ and $\delta^{13}C$ Between Sites U1336, U1337, and U1338

Comparison of the benthic foraminiferal stable isotope records shows close similarity between the three sites, given that the long-term trends as well as the amplitudes and timing of the carbon isotope and climate events agree well.

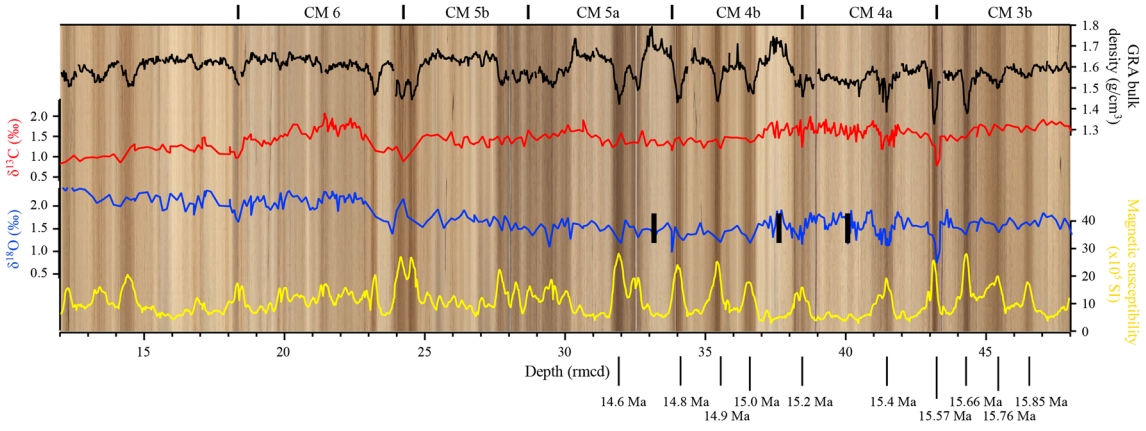

Figure 5. Benthic foraminiferal $\delta^{18}O$ and $\delta^{13}C$, and lithological proxy data of Site U1336 plotted on top of the core splice image from 48 to 12 rmcd (16–13 Ma). Revised depth scale and data for GRA bulk density, magnetic susceptibility, and the splice image are adopted from *Wilkens et al.* [2013]. GRA bulk density data (black) are inversely correlated, and magnetic susceptibility (yellow) is positively correlated with darker colored bands in the sediment. $\delta^{18}O$ (blue) also correlates with the sediment color, unlike $\delta^{13}C$ (red). In the interval from 46.8 to 31.8 rmcd, short eccentricity cycles (100 kyr) correspond to the darker colored bands. The ages of the isotope decreases ($\delta^{18}O$) coinciding with these bands are shown below the *x*-axis. Carbon isotope maxima events (CM) of the Monterey Excursion are given above the splice image and indicate the depth range of each event. Black bars mark the depth, where missing 100 kyr cycles are located. For further explanations, see supporting information Text S1.

The highest $\delta^{13}C$ values of the Monterey Excursion (16.9–13.5 Ma) occurred during the carbon isotope events CM 3b, CM 4a, and CM 6 (Figure 3). The maximum $\delta^{13}C$ values of the three sites range between 1.8 and 2.0‰ during CM 3b and between 1.7 and 2.0‰ during CM 4 [*Tian et al.*, 2013; *Holbourn et al.*, 2014]. During the CM 6 event, the $\delta^{13}C$ values are between 1.8 and 2.1‰ [*Tian et al.*, 2013; *Holbourn et al.*, 2014] (Figure 3).

A marked $\delta^{18}O$ minimum, centered at ~15.6 Ma, can be clearly identified in all three records (Figure 3). This $\delta^{18}O$ minimum was accompanied by a sharp decline in $\delta^{13}C$. The $\delta^{18}O$ values decrease to 0.74‰, 0.63‰, and 0.67‰, the $\delta^{13}C$ values decline to 0.77‰, 0.82‰, and 0.76‰ at Sites U1336, U1337 [*Tian et al.*, 2013], and U1338 [*Holbourn et al.*, 2014], respectively (Figure 3).

Between 13.9 and 13.7 Ma, $\delta^{18}O$ increases rapidly by 0.95‰ at Site U1336, in agreement with the measured changes at Sites U1337 (1.04‰) [*Tian et al.*, 2013] and U1338 (1.32‰) [*Holbourn et al.*, 2014]. The concurring shift in $\delta^{13}C$ is 0.92‰ at Site U1336 and is comparable to 0.88‰ and 0.90‰ at Sites U1337 [*Tian et al.*, 2013] and U1338 [*Holbourn et al.*, 2014], respectively (Figure 3).

Although the $\delta^{18}O$ signatures of Site U1336 are comparable to that of Site U1338 (and Site U1337) throughout the entire investigated interval, discrepancies greater than the 2σ measurement uncertainty exist between the $\delta^{13}C$ records. The U1336 $\delta^{13}C$ record seems more variable within event CM 4 with partially higher values (by up to 0.5‰) between 15.2 and 15.0 Ma, when maxima and minima values are compared between the sites (Figure 3). The $\delta^{13}C$ record also shows increased values compared to Site U1338 between 13.4 and 13.0 Ma with offsets varying between 0.2 and 0.4‰. The $\delta^{13}C$ values of Sites U1336 and U1337 agree well between 15.2 and 15.0 Ma, but the $\delta^{13}C$ values of Site U1336 are higher (by up to 0.5‰) between ~14.5 and 14.0 Ma and between 13.4 and 13.1 Ma (by 0.3‰) (Figure 3). Further, the onset of event CM 6 occurred 40–70 kyr earlier at Site U1337 (13.99 Ma) and at Site U1336 (13.96 Ma) than at Site U1338 (13.92 Ma), but this most likely results from the different tuning approaches applied.

3.4. SEM Imaging of Benthic Foraminiferal Tests of Sites U1336, U1337, and U1338

Under the light microscope, tests of all three sites from 16 to 13 Ma were opaque and no visual distinction could be made between tests from the different sites. However, a few specimens within one sample of Site U1336 appeared poorly preserved compared to the others. SEM images of broken tests and test wall cross sections suggest that tests of all three sites are recrystallized to a certain extent, although tests from the middle Miocene cooling (~13.9 Ma) appear better preserved (not shown here), based on their microgranular texture, than tests from the peak warmth event during the Miocene climate optimum (~15.6 Ma) (Figure 6). Test wall cross sections of all three sites from ~15.6 Ma show micron-sized crystals (red arrows) (Figures 6d and 6e). Calcite overgrowth in the form of bulky micron-sized crystals on the inner and outer surface has been noted for some specimens from ~15.6 Ma at all sites. However, tests from Site U1338 appear better preserved during this time interval than tests from the other sites (Figures 6c and 6f).

4. Discussion

4.1. Comparison of the Carbon Isotope Events

The stable isotope record of Site U1336 exhibits a good agreement with the high-resolution records of Sites U1337 (3–4 kyr) [*Tian et al.*, 2013] and U1338 (1–3 kyr) [*Holbourn et al.*, 2014] (Figure 3). The onset of the carbon isotope excursion CM 4a is marked by a $\delta^{18}O$ minimum and inferred peak warmth episode centered at ~15.6 Ma clearly recognizable in all three records (Figure 3). This abrupt warming was associated with a sharp decline in $\delta^{13}C$ with a similar amplitude as for $\delta^{18}O$ (see section 3.3; Figure 3). The peak warmth interval was also identified at the subtropical Ocean Drilling Program (ODP) Sites 1146 (South China Sea) and 1237 (Nazca Ridge, off Peru) [*Holbourn et al.*, 2005, 2007]. At Site U1338, the pronounced decrease in $\delta^{18}O$ and $\delta^{13}C$ is accompanied by a minimum in carbonate content [*Holbourn et al.*, 2014].

The intense ~1‰ increase in $\delta^{18}O$ at Sites U1336, U1337, and U1338 between ~13.9 and 13.8 Ma marks the onset of the global Miocene cooling and is associated with the onset of event CM 6 [e.g., *Holbourn et al.*, 2005, 2007; *Miller et al.*, 1991; *Shackleton and Kennett*, 1975; *Woodruff and Savin*, 1991]. The covarying benthic $\delta^{18}O$ and $\delta^{13}C$ data of Sites U1336, U1337, and U1338 during the interval 16.0–14.2 Ma (Figure 3) indicate that global ice volume and deep water temperature changes largely coincided with changes in the global carbon

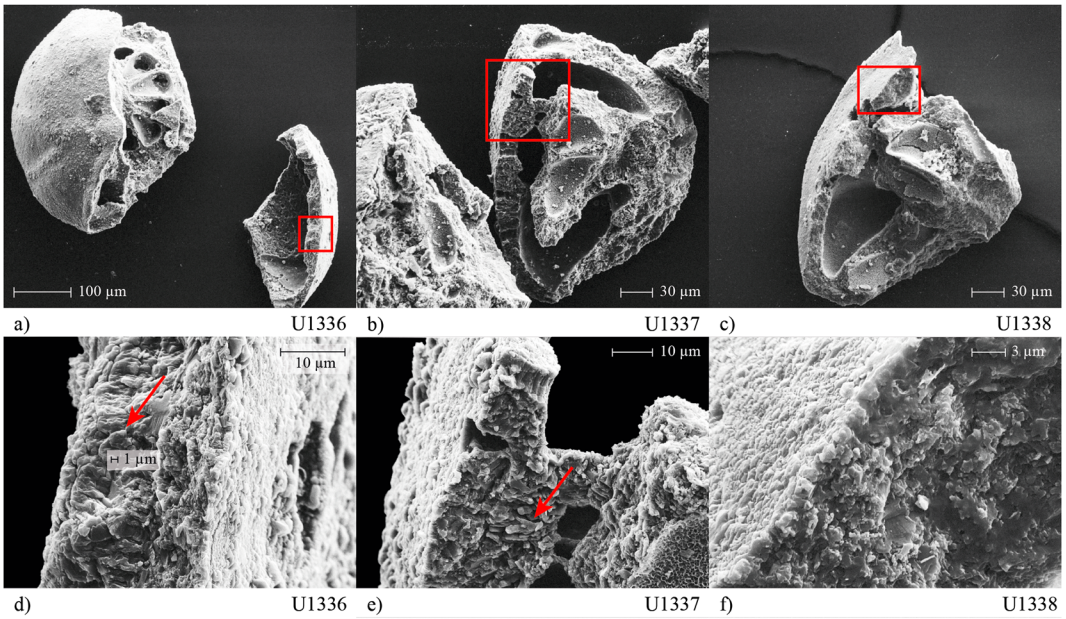

Figure 6. SEM images of broken *C. mundulus* tests from Sites (a, d) U1336, (b, e) U1337, and (c, f) U1338 from sediment sections from ~15.6 Ma. Red squares indicate the location of the wall cross sections of the same tests from Figures 6a–6c. Generally, SEM images suggest that none of the specimens are pristine as the texture of the cross sections show micron-sized crystals (red arrows), indicated by the 1 µm bar in Figure 6d. Preservation seems to be best for Site U1338, and tests from Site U1336 are less well preserved as they also show evidence of secondary calcite overgrowth.

cycle on orbital timescales [e.g., *Flower and Kennett*, 1993, 1994; *Kirtland Turner*, 2014; *Pälike et al.*, 2006; *Ma et al.*, 2011; *Vincent and Berger*, 1985; *Zachos et al.*, 2008, 2010].

The observed deviations in $\delta^{13}C$ values (by comparing maxima and minima values) between Sites U1336, U1337, and U1338, especially during event CM 4 (15.2–15.0 Ma, see section 3.3), may have been caused by small changes in productivity due to different paleolatitudes (see Figure 1). These offsets may also result from different tuning approaches and/or different resolution of the isotope records as the temporal resolution of Site U1336 is lower compared to the other sites, therefore possibly missing smaller events. The $\delta^{13}C$ values of Sites U1337 and U1338 do not differ markedly, except for the time intervals 14.96–14.85 Ma and 14.24–14.13 Ma, the latter difference most likely resulting from the different age models used (Figure 3). Both sites were still in the equatorial zone of high primary productivity during the entire investigated time interval (Figure 1) [*Pälike et al.*, 2010], which possibly resulted in consistency between the $\delta^{13}C$ data due to similar productivity in the upper ocean. In contrast, Site U1336 traveled out of the high-productivity zone at ~23 Ma (see also Figure 1) [*Pälike et al.*, 2010], resulting in decreased surface water production above Site U1336 in comparison to the other sites. In general, the benthic $\delta^{13}C$ signal is influenced by local primary productivity and deep water circulation in addition to changes in the global carbon reservoir [e.g., *Belanger et al.*, 1981; *McCorkle et al.*, 1995]. Due to the proximity of the three sites, deep water circulation can be assumed to be identical at the sites, which is confirmed by similar deep water $\delta^{13}C$ values [e.g., *Key et al.*, 2004; *Kroopnick*, 1985]. However, at the water sediment interface $\delta^{13}C$ can be quite different due to the remineralization of organic material. In general, organic material, formed in the mixed layer, is depleted in ^{13}C and when it sinks to the deep ocean, it is remineralized lowering the $\delta^{13}C$ of the inorganic carbon pool of the deep ocean and at the water sediment interface [e.g., *Mackensen et al.*, 1993; *McCorkle et al.*, 1995; *Woodruff and Savin*, 1991]. The remineralization of organic matter can result in lower $\delta^{13}C$ values of benthic foraminiferal tests (by up to ~0.6‰) underneath high-productivity zones compared to areas with less surface production [e.g., *Mackensen et al.*, 1993]. Less ^{13}C-depleted carbon may have been incorporated into benthic foraminiferal tests of Site U1336 resulting in elevated benthic $\delta^{13}C$ values compared to the values from Sites U1337 and U1338. The observed positive offset in $\delta^{13}C$ values between Sites U1336 and U1338 during 15.2–15.0 Ma (Figure 3) could also result from carbonate dissolution and subsequent early recrystallization because recrystallized tests tend to have elevated $\delta^{13}C$ values compared to well-preserved contemporaneous tests [e.g., *Pearson et al.*, 2001; *Sexton*

et al., 2006]. This, in turn, would imply that Site U1337 is also recrystallized for that time interval, since the $\delta^{13}C$ values of Sites U1336 and U1337 show similar values, although shipboard analysis of Site U1337 indicated good test preservation and SEM images (Figures 6b and 6e) also suggest at least moderate preservation. Even though the possibility of recrystallization affecting the $\delta^{13}C$ values cannot entirely be ruled out, it seems unlikely that detectable changes in $\delta^{13}C$ only occurred in this interval. Therefore, slight offsets (up to 0.4–0.5‰ in $\delta^{13}C$) caused by decreased primary productivity are the best explanation for the small deviations in $\delta^{13}C$ between Sites U1336 and U1338.

4.2. Robustness of Benthic Foraminiferal Stable Isotopes as Paleoceanographic Proxies

In addition to the similar shifts in timing and magnitudes of the Site U1336 benthic foraminiferal stable isotope record to those of the better preserved sites nearby (Figure 3), even the finer details of the stable isotope record agree well with high-resolution records of Sites U1337 [*Tian et al.*, 2013] and U1338 [*Holbourn et al.*, 2014] (Figure 3) and the high-resolution record (~4–9 kyr) of the subtropical ODP Site 1237 [*Holbourn et al.*, 2005, 2007]. However, the $^{87}Sr/^{86}Sr$ ratio of bulk sediments at Site U1336 suggests active recrystallization in the sediment column below 100 rmcd ($>$ 20 Ma) [*Voigt et al.*, 2015]. Between 14.7 and 12.5 Ma, the U1336 bulk carbonate Sr/Ca ratios are ~1.80 mmol/mol but decrease to an average of 1.37 mmol/mol between 16.0 and 15.3 Ma (Figure S7) [*Voigt et al.*, 2015]. This low value is comparable to the more recrystallized ODP Sites 806 and 807 with contemporaneous average bulk carbonate Sr/Ca ratios of 1.46 and 1.41 mmol/mol, respectively (Figure S7) [*Delaney and Linn*, 1993], indicating geochemical alteration of the bulk carbonates of U1336 between 16.0 and 15.3 Ma (Figure S7) [*Voigt et al.*, 2015]. SEM images imply that the benthic foraminiferal tests of the Sites U1336–U1338 are recrystallized to a certain extent within this interval (Figure 6); however, we find similar benthic foraminiferal stable isotope values (within 2σ measurement uncertainty) between the sites (Figure 3), suggesting minor alteration of the geochemical signatures of benthic tests.

Based on benthic foraminiferal stable isotope data from Oligocene sections (~30-33 Ma) from the eastern equatorial Pacific close to the sites investigated here, *Edgar et al.* [2013] suggested that recrystallization occurred relatively quickly ($<$ 10 Ma) after burial at shallow depths ($<$ 100 m) to maintain the original geochemical signal. This hypothesis is confirmed in the upper sections of Site U1336 where the radiogenic Sr isotope ($^{87}Sr/^{86}Sr$) data suggest fast recrystallization of bulk carbonates (within ~1.5 Ma) after burial (Figure S1) [*Voigt et al.*, 2015]. In order to preserve the original $\delta^{18}O$ and $\delta^{13}C$ signals, the benthic foraminiferal tests possibly recrystallized in a water mass similar to that during calcification, as the uppermost pore waters have a temperature and isotopic composition similar to bottom seawater [*Edgar et al.*, 2013; *Pearson et al.*, 2001; *Schrag*, 1999; *Schrag et al.*, 1995]. On the other hand, the orbital scale similarity of the benthic foraminiferal stable isotope values of the investigated sites implies that the tests recrystallized on much faster timescales (within $<$ 100 kyr), confirmed by the preservation of orbital cyclicity (100 kyr and 400 kyr) at Site U1336 (Figures 2 and 4). Recrystallization of the tests in sediment depths below diffusive exchange with bottom seawater and pore waters (~5–10 m at Sites U1336–U1338, corresponding to ~1–3 Myr) would result in much lower $\delta^{18}O$ values (see Table 1, late recrystallization). Although it is still debated whether biogenic and inorganic carbonates precipitate in isotopic equilibrium with seawater, pore waters, in which recrystallization occurs, possibly reflect $\delta^{18}O$ and $\delta^{13}C$ equilibrium conditions, since pore water processes are thought to be very slow and thus are close to isotopic equilibrium [e.g., *Dietzel et al.*, 2009; *Kim and O'Neil*, 1997; *McCrea*, 1950; *O'Neil et al.*, 1969; *Zeebe*, 1999; *Zeebe et al.*, 1999]. This is supported by Ca isotope data, which suggests conditions close to equilibrium with pore waters, meaning no kinetic effects [e.g., *Böhm et al.*, 2012; *DePaolo*, 2011; *Fantle and DePaolo*, 2007]. In Table 1, the composition of secondary inorganic calcite that would precipitate from Site U1336 pore waters during the middle Miocene was estimated. Using these values, the amount of geochemical alteration that is needed to detect a change in the benthic foraminiferal isotope composition was calculated (see Table captions and section 2.3). The recrystallized $\delta^{18}O$ composition was estimated following two scenarios: (1) early recrystallization within the first 1–3 Myr in shallow depths near bottom waters and (2) a late phase of recrystallization in sediments older than 10 Ma, as observed at Site U1336 [*Voigt et al.*, 2015], using pore water $\delta^{18}O$ data from nearby sites [*Lawrence et al.*, 1975]. Three time intervals were chosen and represent the Middle Miocene Climate Optimum with low $\delta^{18}O$ values (16.0–15.2 Ma), the Miocene cooling event with ~1‰ increase in the $\delta^{18}O$ values (13.9–13.8 Ma), and the subsequent cold icehouse mode (13.5–13.2 Ma). For simplicity, it is assumed that the secondary

Paleoceanography
10.1002/2015PA002822

Table 1. Calculated Composition of Recrystallized Calcite[a]

	Time Slice (Ma)	Bottom Seawater T (°C)[b]	$\delta^{18}O$ Seawater (‰ VSMOW)[b]	$\delta^{18}O$ Fractionation Factor[c]	$\delta^{18}O$ Inorganic Calcite (‰ VPDB)[d]	$\delta^{18}O$ Primary Calcite (‰)[e]	Percentage Recrystallized $\delta^{18}O$ (%) to Shift by 0.24‰[f]	$\delta^{18}O$ Recrystallized (‰)[f]	Average $\delta^{18}O$ (‰) of Site U1336
Early recrystallization	13.5–13.2	8.7	0.720	1.0321	1.88	1.99	-	-	2.06
	13.9–13.8	9.1	0.630	1.0320	1.71	1.91	-	-	2.12
	13.9–13.8	9.1	0.766	1.0320	1.84	1.91	-	-	2.12
	16.0–15.2	10.2	0.401	1.0317	1.23	1.51	85	1.27	1.56
	Time Slice (Ma)	Estimated *T* (°C)[g]	Measured $\delta^{18}O$ Pore Water (‰ VSMOW)[h]	$\delta^{18}O$ Fractionation Factor[c]	$\delta^{18}O$ Inorganic Calcite (‰ VPDB)[d]	$\delta^{18}O$ Primary Calcite (‰)[e]	Percentage Recrystallized $\delta^{18}O$ (%) to Shift by 0.24‰[f]	$\delta^{18}O$ Recrystallized (‰)[f]	Average $\delta^{18}O$ (‰) of Site U1336
Late phase of recrystallization	13.5–13.2	7.6	−1.25	1.0323	0.16	1.99	13	1.75	2.06
	13.9–13.8	11.2	−2.00	1.0315	−1.41	1.91	7.2	1.67	2.12
	16.0–15.2	13.7	−1.70	1.0309	−1.66	1.51	7.5	1.27	1.56
	16.0–15.2	7.6	−0.50	1.0323	0.91	1.51	40	1.27	1.56
	Time Slice (Ma)	Bottom Water T (°C)[b]			$\delta^{13}C$ Inorganic Calcite (‰)[i]	$\delta^{13}C$ Primary Calcite (‰)[e]	Percentage Recrystallized $\delta^{13}C$ (%) to Shift by 0.18‰[f]	$\delta^{13}C$ Recrystallized (‰)[f]	Average $\delta^{13}C$ (‰) of Site U1336
	13.5–13.2	8.7			-	0.97	-	-	1.22
	13.9–13.8	9.1			2.07	1.25	22	1.43	1.66
	16.0–15.2	10.2			2.16	1.54	29	1.72	1.61

[a]The amount of recrystallization was calculated that is required to alter benthic foraminiferal stable isotope values detectably (above 2σ measurement uncertainty). Please note the different order of the time intervals for early and late recrystallization. See text for explanations of early and late recrystallization as well as time intervals.

[b]Bottom water temperatures and $\delta^{18}O$ data of seawater were taken from *Lear et al.* [2010], averaged for the time slices, and $\delta^{18}O$ was converted to the VSMOW scale by using the equation $\delta^{18}O(VSMOW) = \delta^{18}O(VPDB) + 0.27‰$ [*Hut*, 1987].

[c]Fractionation factors for the temperatures given were calculated using the equation from *Kim and O'Neil* [1997].

[d]$\delta^{18}O$ of inorganic calcite was calculated using the equation: $\delta^{18}O_{calcite}(VSMOW) = \text{fractionation factor } \alpha\ (\delta^{18}O_{seawater}(VSMOW) + 1000) - 1000$ and the $\delta^{18}O$ of seawater or pore water and fractionation factors in columns 4 and 5. The calculated $\delta^{18}O_{calcite}$ was converted to the VPDB scale by $\delta^{18}O_{calcite}(VPDB) = (\delta^{18}O_{calcite}(VSMOW) - 30.86)/1.03086$ [*Hoefs*, 2009].

[e]The stable isotope values are averages for each time slice using the record from *Holbourn et al.* [2014] assuming good preservation.

[f]Percentages and composition of recrystallized stable isotopes were calculated by $\delta i_{recrystallized} = (\delta i_{inorganic\ calcite} * x) + (\delta i_{primary\ calcite} * 1 - x)$ where x is the fraction of inorganic calcite precipitated during recrystallization.

[g]Estimated temperatures for the depths of the pore water samples from Deep Sea Drilling Project (DSDP) Sites 71 and 72 from *Lawrence et al.* [1975] (column 4) using the geothermal gradient of those sites [*Von Herzen et al.*, 1971].

[h]Measured $\delta^{18}O$ values of pore waters from DSDP Sites 71 and 72, data are from *Lawrence et al.* [1975].

[i]Bulk carbonate $\delta^{13}C$ (‰) is used as $\delta^{13}C$ of inorganic calcite. Data used for the time slice 13.9–13.8 Ma are from *Pälike et al.* [2006] from the Mi-1 glaciation (~23 Ma) assuming similar values during the major cooling step at 13.9–13.8 Ma. Data used for the time slice 16.0–15.2 Ma are averages from 16.2 to 15.5 Ma from *Holbourn et al.* [2015]. These values of $\delta^{13}C$ = ~2‰ are in good agreement with $\delta^{13}C$ model and experimental studies [e.g., *Mook*, 1986; *Walter et al.*, 2007; *Zeebe et al.*, 1999].

calcite is formed in isotopic equilibrium with the fluids that it precipitated from. The average benthic stable isotope signature of Site U1338 [*Holbourn et al.*, 2014] during each time slice was adopted to represent primary biogenic calcite. The $\delta^{18}O$ values of inorganic calcite that would precipitate from the uppermost pore waters during early recrystallization are similar (within 2σ measurement uncertainty) to the primary foraminiferal $\delta^{18}O$ values for the time intervals 13.5–13.2 Ma and 13.9–13.8 Ma. During the time interval 16.0–15.2 Ma, a high percentage of inorganic calcite (85%) is needed to change the benthic $\delta^{18}O$ values above measurement uncertainties. These results confirm that recrystallization could have occurred very rapidly after burial (<100 kyr, see section 4.1) because even complete recrystallization of the benthic tests results in negligible alteration (within 2σ measurement uncertainty) of the $\delta^{18}O$ signatures, except for the time interval 16.0–15.2 Ma (Table 1). For any late stage recrystallization, the difference between inorganic calcite and benthic foraminiferal $\delta^{18}O$ values is large (0.6–3.3‰), so the percentage of recrystallized calcite needed to change the benthic $\delta^{18}O$ values detectably (by 2σ measurement uncertainty) is small (between 7.2% and 13%) for the time intervals 13.5–13.2 Ma and 13.9–13.8 Ma (Table 1). The difference between U1338 (primary calcite values in Table 1) and U1336 $\delta^{18}O$ values cannot be explained by the addition of inorganic calcite during early or late recrystallization as the average U1336 $\delta^{18}O$ values are higher than the estimated recrystallized $\delta^{18}O$ composition. It is possible that the temperature and bottom water $\delta^{18}O$ data used to calculate the inorganic calcite composition are not entirely appropriate (data are from ODP Site 761, off northwest Australia [*Lear et al.*, 2010], which were still in exchange with Pacific waters during the middle Miocene), but no data for the middle Miocene exist from the equatorial Pacific. Despite this, the benthic isotope data from Site U1338 can be assumed to represent primary calcite as they agree well with the benthic Pacific trend data of *Cramer et al.* [2009] for the time slices investigated, except for 16.0–15.2 Ma, where the U1338 $\delta^{18}O$ values are higher by 0.2‰, possibly caused by lower temperatures in the upwelling area. The average $\delta^{13}C$ values of Site U1336 are higher than those of U1338 (primary calcite) and therefore suggest detectable recrystallization of 22% and 29% for the time intervals 13.9–13.8 Ma and 16.0–15.2 Ma, respectively (Table 1). However, the $\delta^{18}O$ values indicate very good preservation of the geochemical signature of the U1336 tests, and $\delta^{18}O$ is more sensitive to recrystallization than $\delta^{13}C$ [e.g., *McCorkle et al.*, 1995; *Pearson et al.*, 2001; *Sexton et al.*, 2006]. Therefore, this discrepancy between the $\delta^{13}C$ values of Sites U1336 and U1338 might be explained by their geographic location and thus different surface productivity during the time intervals instead of recrystallization (see section 4.1). Nevertheless, it is surprising that the amount of recrystallization required to shift the $\delta^{18}O$ detectably is the highest at the time interval 16.0–15.2 Ma for both scenarios (85 and 40%, Table 1). This might suggest low contribution of inorganic calcite during this time interval, although the Sr proxies of the bulk sediment and pore waters (Sr/Ca and $^{87}Sr/^{86}Sr$ ratios) show increased recrystallization in sediments older than 14.7 Ma (Figures S1 and S7) [*Voigt et al.*, 2015]. Further, SEM images of the benthic foraminiferal tests of Site U1336 clearly show some degree of recrystallization indicating that the tests from Site U1336 are less well preserved compared to tests from Site U1338 (Figure 6) (see section 3.4); nevertheless, the stable isotope data suggest negligible intersite offsets (Table 1). This lack of intersite offsets regarding timing and amplitudes of isotopic changes, further implies minimal geochemical alteration of the isotopes during early stage recrystallization as diagenetic alteration is expected to reduce the amplitude of stable isotope signatures similar to diminishing interspecies differences in stable isotope values [e.g., *Pearson et al.*, 2001, 2007]. These results suggest that benthic foraminiferal tests preserve the original geochemical signature during the investigated time intervals (16–13 Ma). Therefore, only minor, if any, geochemical alteration of the stable isotope signatures occurred early after burial (within <100 kyr, corresponding to 1.2–4.7 m) at very shallow sediment depths. However, it cannot be ruled out that benthic foraminiferal stable isotope compositions of Site U1336 are more severely affected by recrystallization in the deeper, more active sediment section (>100 m, corresponding to >20 Ma).

Edgar et al. [2013] suggested that burial depth and sedimentation rates do not influence the diagenetic alteration of benthic foraminiferal stable isotopes. The difference in burial depth between the shallowest (U1336, 192 rmcd) and the deepest buried site (U1337, 498 rmcd) is larger than at the sites investigated by *Edgar et al.* [2013]. Similar to the sites studied by *Edgar et al.* [2013], the lithologies of the sites investigated here consist of mainly nannofossil ooze (see section 2.1) with some chalky intervals within the lower sections of Sites U1337 and U1338 [*Pälike et al.*, 2010]. Sites U1337 and U1338 experienced higher sedimentation rates than U1336 [*Pälike et al.*, 2010], but the $\delta^{18}O$ data of all three sites are nevertheless in good agreement (Figure 3) confirming little influence of burial depth on these benthic stable isotope data. In contrast to the

previous study by *Edgar et al.* [2013], the resolution of the records compared here is higher reaching 9 kyr on average for Site U1336 compared to 20 kyr. This higher temporal resolution allows a more detailed comparison of the stable isotopes between the sites and shows a good agreement throughout the entire studied time interval. Although the sites investigated by *Edgar et al.* [2013] comprise older sediments (Eocene–Oligocene) and are thus comparable to Site U1336, the bulk carbonate radiogenic Sr isotopes of Site U1334, one of the sites studied by the authors, do not suggest a late stage of recrystallization as observed at Site U1336 [*Voigt et al.*, 2015]. In addition, several Sr parameters (including $^{87}Sr/^{86}Sr$, $\delta^{88/86}Sr$, and Sr/Ca) indicate that Site U1336 bulk carbonates are more extensively altered than those at Site U1334 [*Voigt et al.*, 2015]. The fact that Sites U1334 and U1336 are of similar age but have different diagenetic histories strengthens the finding that foraminiferal stable isotope signatures are only slightly influenced by diagenetic alteration [see also *Edgar et al.*, 2013] even in the severely altered sediment sections of Site U1336. However, this needs to be tested further in older sediments at Site U1336.

Another parameter that is expected to change the foraminiferal $\delta^{18}O$ signature of calcite as it recrystallizes is the geothermal gradient (see also Table 1). Oxygen isotope fractionation is temperature dependent, resulting in lower $\delta^{18}O$ values at higher temperatures with a decrease in the fractionation factor by 0.00023 per Kelvin [e.g., *Kim and O'Neil*, 1997]. The geothermal gradients of Sites U1337 and U1338 are similar, showing values of 32.4°C/km and 34.4°C/km, respectively [*Pälike et al.*, 2010]. Unfortunately, no in situ temperatures were measured at Site U1336 but a comparison of pore water Mg/Ca gradients with other sites in the region suggests a much steeper thermal gradient for Site U1336 (~79°C/km), which is considered to be the primary driver of carbonate recrystallization at this site [*Voigt et al.*, 2015]. Bulk carbonates of Site U1336 are more altered due to the influence of the high geothermal gradient [*Voigt et al.*, 2015], although the Miocene section has a shallower burial depth compared to the other sites [*Pälike et al.*, 2010]. Nevertheless, the U1336 $\delta^{18}O$ data are similar to the U1337 and U1338 $\delta^{18}O$ records (Table 1 and Figure 3). Furthermore, the temperature range for the investigated depth interval at Site U1336 is 2.4–5.3°C using the geothermal gradient and the bottom temperature of 1.46°C in the study area [*Pälike et al.*, 2010], whereas the sediment temperatures of the depth range corresponding to the time interval 16–13 Ma are twofold to threefold higher at Sites U1337 and U1338 [*Pälike et al.*, 2010]. Therefore, chemical alteration of tests from these two sites would result in lower $\delta^{18}O$ values (by ~1.4–2.5‰) compared to Site U1336 during the investigated time interval, which is not observed. Therefore, any influence of the geothermal gradient on $\delta^{18}O$ and $\delta^{13}C$ signatures was obviously too small to cause any significant changes in the isotopic compositions of the benthic foraminiferal tests.

4.3. Integrating Magnetostratigraphy and Isotope Stratigraphy

Unfortunately, the paleomagnetic signal of Sites U1337 and U1338 was compromised during the mid-Miocene by reductive diagenesis, possibly by the dissolution of magnetite [*Pälike et al.*, 2010]. Our new benthic stable isotope data allow the well-resolved paleomagnetic stratigraphy of Site U1336 to be transferred to Sites U1337 and U1338 by correlating the U1336 stable isotope stratigraphy to those sites (Table S3 and Figure 3). To assess the reliability of this, we compare the independent orbital tuning of Site U1336 (color reflectance b*) (orbital age model hereafter) with the age model based on paleomagnetic data ("Chron" age model hereafter) [*Ohneiser et al.*, 2013] (Figure 7; see also supporting information Text S2). The orbital tuning of color reflectance b* can be directly related to the benthic foraminiferal stable isotopes since the changes in the isotope record are reflected in the lithology of the succession (see supporting information Text S1). The Chron age model for the interval 16–13 Ma relies on relatively few reversals and thus cannot rival the fidelity of orbitally tuned, high-resolution records, such as the foraminiferal stable isotopes of Sites U1337 and U1338 or the color reflectance of Site U1336. This may explain the discrepancies between the Chron and orbital age model resulting in offsets ranging from 32 to 171 kyr (Table S2 and Figure 7). A recent study showed that the $CaCO_3$ content data of Site U1336 were offset by ~100 kyr at ~17 Ma, when adjusted to the Chron age model from *Ohneiser et al.* [2013] [*Keegan Wilson*, 2014, see Figure 13 therein]. Only two magnetic age points exist between 15.9 and 15.2 Ma (Table S2), suggesting constant sedimentation rates within this time interval which clearly does not agree with the detailed sedimentation rates derived from the orbital age model resulting in large offsets within this interval (Figure 7; see also supporting information Text S2). The largest differences between the age models occur within Chrons C5Bn.2n-C5ADn (15.2–14.2 Ma) (Figure 7), where the magnetostratigraphy is less well constrained due to different possible calibrations

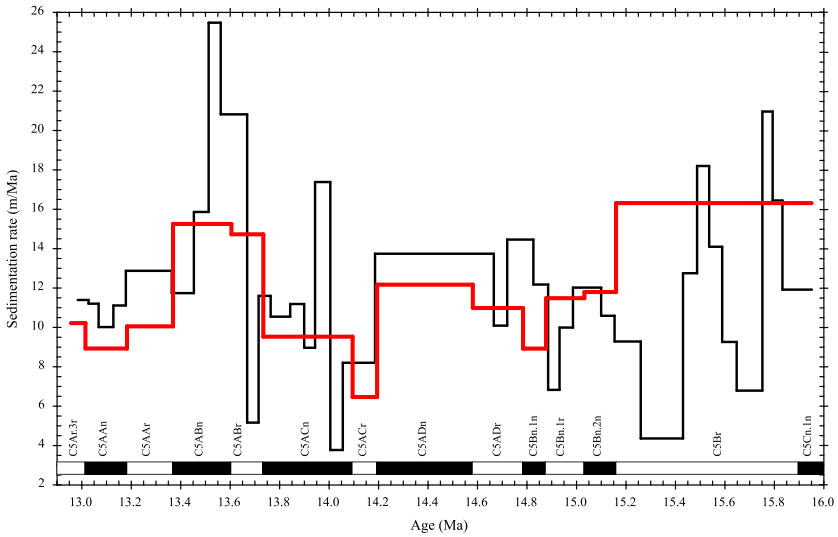

Figure 7. Comparison of the calculated sedimentation rates of Site U1336 based on the age model of color reflectance b* (black) and the age model derived from paleomagnetic data (red) [*Ohneiser et al.*, 2013]. The polarity stratigraphy of Site U1336, based on paleomagnetic data [*Ohneiser et al.*, 2013; *Pälike et al.*, 2010], is given for comparison.

[*Ohneiser et al.*, 2013]. The time interval thereafter (14.2–13.0 Ma) has lower offsets with an average of 83 kyr suggesting a better correlation between the age models (Table S2) except for the short intervals at 14.0–13.9 Ma and 13.7–13.5 Ma, where the sedimentation rates markedly differ (Figure 7; see also supporting information Text S2). These differences between the models most likely result from the amount and choice of tie points but also suggest that high-resolution stable isotopes and color reflectance records are more sensitive to regional and global events. However, considering these caveats resulting in uncertainties of ~100 kyr, the overall good agreement between the stable isotope records allows the mid-Miocene magnetostratigraphy of Site U1336 to be transferred to Sites U1337 and U1338.

5. Conclusions

Although the bulk sediments of Site U1336 show increased and persistent recrystallization in sediments older than 14.7 Ma, the benthic foraminiferal stable isotope record is in good agreement with high-resolution records in better preserved sediment successions at Sites U1337 and U1338. All carbon isotope events of the Monterey Excursion can be clearly identified within the investigated interval (16–13 Ma). The absolute values and amplitudes of $\delta^{18}O$ and $\delta^{13}C$ signatures compare well with those from the neighboring Sites U1337 and U1338. Long eccentricity cycles (400 kyr) are clearly evident in the $\delta^{13}C$ record and within the interval of 15.5–14.7 Ma even the short eccentricity cycles (100 kyr) can be distinguished. The close resemblance of the new stable isotope data of Site U1336 to the records of Sites U1337 and U1338 allows the well-resolved paleomagnetic results of Site U1336 [*Ohneiser et al.*, 2013] to be transferred to Sites U1337 and U1338 improving the global geological timescale. Benthic foraminiferal stable isotope signatures of Site U1336 experienced no detectable effect from recrystallization indicating that benthic foraminifera preserved much of the original geochemical signal despite recrystallization of the bulk sediments and to a lesser extent of the benthic foraminiferal tests. This can be explained by extremely fast recrystallization (within $<$ 100 kyr) after burial at shallow sediment depths as the orbital cyclicity (100 kyr and 400 kyr cycles) is still preserved at Site U1336, whereas recrystallization of the tests over longer timescales would reduce the signal power of these cycles. The tests must have recrystallized in the uppermost pore waters, which have a temperature and isotopic composition similar to bottom seawater, resulting in negligible offsets from primary $\delta^{18}O$ and $\delta^{13}C$ values. Therefore, benthic foraminifera in carbonate-rich sediments of Miocene age and younger can reliably be used for isotope analyses, establishment of stratigraphies, and paleoceanographic reconstructions.

Acknowledgments
This work was funded by the German Science Foundation, DFG, HA 5751/1-1 and HA 5751/2-1 (PEAT). The manuscript was greatly improved by the comments of Phil Sexton and one anonymous reviewer. We thank Isabel Rohr and Julia Langer for preparing the samples and help picking the benthic foraminifera. We further thank Lulzim Haxhiaj, Kirstin Werner, Christelle Not, Andrea Bodenbinder, and Fynn Wulf for measuring the stable isotopes. Roy Wilkens kindly provided the U1336 splice image, and the data for GRA bulk density and magnetic susceptibility. We also thank Jacek Raddatz, Daniel Gebrigeorgis Yirgaw, and Dirk Nürnberg for help with AnalySeries. Steffanie Kraft is acknowledged for helpful discussions at an early stage of the manuscript. The U1336, U1337 [*Tian et al.*, 2013], and U1338 [*Holbourn et al.*, 2015] data sets can be found on the Pangaea database at http://www.pangaea.de.

References

Baker, P. A., J. M. Gieskes, and H. Elderfield (1982), Diagenesis of carbonates in deep-sea sediments-evidence from Sr/Ca ratios and interstitial dissolved Sr^{2+} data, *J. Sediment. Petrol.*, *52*, 71–82.

Belanger, P. E., W. B. Curry, and R. K. Matthews (1981), Core-top evaluation of benthic foraminiferal isotopic ratios for paleo-oceanographic interpretations, *Paleogeogr. Paleoclimatol. Paleoecol.*, *33*(1–3), 205–220, doi:10.1016/0031-0182(81)90039-0.

Blum, P. (1997), Reflectance, spectrophotometry and colorimetry, in Physical Properties Handbook: A guide to the shipboard measurement of physical properties of deep-sea cores, *ODP Tech. Note*, 26, doi:10.2973/odp.tn.26.1997.

Böhm, F., A. Eisenhauer, J. Tang, M. Dietzel, A. Krabbenhöft, B. Kisakürek, and C. Horn (2012), Strontium isotope fractionation of planktic foraminifera and inorganic calcite, *Geochim. Cosmochim. Acta*, *93*, 300–314, doi:10.1016/j.gca.2012.04.038.

Bown, P. R., et al. (2008), A Paleogene calcareous microfossil Konservat-Lagerstätte from the Kilwa Group of coastal Tanzania, *Geol. Soc. Am. Bull.*, *120*(1–2), 3–12, doi:10.1130/B26261.1.

Cramer, B. S., J. R. Toggweiler, J. D. Wright, M. E. Katz, and K. G. Miller (2009), Ocean overturning since the Late Cretaceous: Inferences from a new benthic foraminiferal isotope compilation, *Paleoceanography*, *24*, PA4216, doi:10.1029/2008PA001683.

Delaney, M. L. (1989), Temporal changes in interstitial water chemistry and calcite recrystallization in marine sediments, *Earth Planet. Sci. Lett.*, *95*(1–2), 23–37, doi:10.1016/0012-821X(89)90165-9.

Delaney, M. L., and L. J. Linn (1993), Interstitial water and bulk calcite chemistry, Leg 130, and calcite recrystallization, in *Proc. ODP. Sci. Results, 130*, edited by W. H. Berger et al., pp. 561–572, Ocean Drilling Program, College Station, Tex.

DePaolo, D. J. (2011), Surface kinetic model for isotopic and trace element fractionation during precipitation of calcite from aqueous solutions, *Geochim. Cosmochim. Acta*, *75*(4), 1039–1056, doi:10.1016/j.gca.2010.11.020.

Dietzel, M., J. Tang, A. Leis, and S. J. Köhler (2009), Oxygen isotopic fractionation during inorganic calcite precipitation—Effects of temperature, precipitation rate and pH, *Chem. Geol.*, *268*, 107–115, doi:10.1016/j.chemgeo.2009.07.015.

Drury, A. J., G. P. Lee, G. M. Pennock, and C. M. John (2014), Data report: Late Miocene to early Pliocene coccolithophore and foraminiferal preservation at Site U1338 from scanning electron microscopy, in *Proc. IODP, 320/321: Tokyo*, edited by H. Pälike et al., Integrated Ocean Drilling Program Management International, Inc., doi:10.2204/iodp.proc.320321.218.2014.

Edgar, K. M., H. Pälike, and P. A. Wilson (2013), Testing the impact of diagenesis on the $\delta^{18}O$ and $\delta^{13}C$ of benthic foraminiferal calcite from a sediment burial depth transect in the equatorial Pacific, *Paleoceanography*, *28*, 468–480, doi:10.1002/palo.20045.

Elderfield, H., and J. M. Gieskes (1982), Sr isotopes in interstitial waters of marine sediments from Deep Sea Drilling Project cores, *Nature*, *300*(5892), 493–497, doi:10.1038/300493a0.

Fantle, M. S., and D. J. DePaolo (2007), Ca isotopes in carbonate sediment and pore fluid from ODP Site 807A: The Ca^{2+}(aq)-calcite equilibrium fractionation factor and calcite recrystallization rates in Pleistocene sediments, *Geochim. Cosmochim. Acta*, *71*(10), 2524–2546, doi:10.1016/j.gca.2007.03.006.

Feldmann, G. C. (2014), Monthly chlorophyll concentration map, June 2012–2014, Map *V20121532014181.L3m*, NASA Ocean Color Web.

Flower, B. P., and J. P. Kennett (1993), The middle Miocene ocean/climate transition: High-resolution oxygen and carbon isotopic records from DSDP Site 588A, southwest Pacific, *Paleoceanography*, *8*(6), 811–843, doi:10.1029/93PA02196.

Flower, B. P., and J. P. Kennett (1994), The middle Miocene climatic transition: East Antarctic ice sheet development, deep ocean circulation and global carbon cycling, *Paleogeogr. Paleoclimatol. Paleoecol.*, *108*(3–4), 537–555, doi:10.1016/0031-0182(94)90251-8.

Fox, L. R., and B. S. Wade (2013), Systematic taxonomy of early-middle Miocene planktonic foraminifera from the equatorial Pacific Ocean: Integrated Ocean Drilling Program, Site U1338, *J. Foramin. Res.*, *43*(4), 374–405.

Gieskes, J. M., H. Elderfield, and M. R. Palmer (1986), Strontium and its isotopic composition in interstitial waters of marine carbonate sediments, *Earth Planet. Sci. Lett.*, *77*(2), 229–235, doi:10.1016/0012-821X(86)90163-9.

Hodell, D. A., G. D. Kamenov, E. C. Hathorne, J. C. Zachos, U. Röhl, and T. Westerhold (2007), Variations in the strontium isotope composition of seawater during the Paleocene and early Eocene from ODP Leg 208 (Walvis Ridge), *Geochem. Geophys. Geosyst.*, *8*, Q09001, doi:10.1029/2007GC001607.

Hoefs, J. (2009), *Stable Isotope Geochemistry*, Springer, Berlin.

Holbourn, A., W. Kuhnt, S. Clemens, W. Prell, and N. Andersen (2013), Middle to late Miocene stepwise climate cooling: Evidence from a high-resolution deep water isotope curve spanning 8 million years, *Paleoceanography*, *28*, 688–699, doi:10.1002/2013PA002538.

Holbourn, A., W. Kuhnt, M. Lyle, L. Schneider, O. Romero, and N. Andersen (2014), Middle Miocene climate cooling linked to intensification of eastern equatorial Pacific upwelling, *Geology*, *42*(1), 19–22, doi:10.1130/G34890.1.

Holbourn, A., W. Kuhnt, K. G. D. Kochhann, N. Andersen, and K. J. S. Meier (2015), Global perturbation of the carbon cycle at the onset of the Miocene Climate Optimum, *Geology*, *43*(2), 123–126, doi:10.1130/G36317.1.

Holbourn, A. E., W. Kuhnt, M. Schulz, and H. Erlenkeuser (2005), Impacts of orbital forcing and atmospheric CO_2 on Miocene ice-sheet expansion, *Nature*, *438*, 483–487, doi:10.1038/nature04123.

Holbourn, A. E., W. Kuhnt, M. Schulz, J.-A. Flores, and N. Andersen (2007), Orbitally-paced climate evolution during the middle Miocene "Monterey" carbon-isotope excursion, *Earth Planet. Sci. Lett.*, *261*(3–4), 534–550, doi:10.1016/j.epsl.2007.07.026.

Hut, G. (1987), Consultants group meeting on stable isotope reference samples for geochemical and hydrological investigations, Report to the Director General, IAEA, Vienna, Austria.

Keegan Wilson, J. (2014), Early Miocene carbonate dissolution in the eastern equatorial Pacific, PhD thesis, Dep. of Oceanography, Texas A&M Univ., College Station, Tex.

Key, R. M., A. Kozyr, C. L. Sabine, K. Lee, R. Wanninkhof, J. L. Bullister, R. A. Feely, F. J. Millero, C. Mordy, and T.-H. Peng (2004), A global ocean carbon climatology: Results from Global Data Analysis Project (GLODAP), *Global Biogeochem. Cycles*, *18*, GB4031, doi:10.1029/2004GB002247.

Kim, S. T., and J. R. O'Neil (1997), Equilibrium and nonequilibrium oxygen isotope effects in synthetic carbonates, *Geochim. Cosmochim. Acta*, *61*(16), 3461–3475, doi:10.1016/S0016-7037(97)00169-5.

Kirtland Turner, S. (2014), Pliocene switch in orbital-scale carbon cycle/climate dynamics, *Paleoceanography*, *29*, 1256–1266, doi:10.1002/2014PA002651.

Kozdon, R., D. C. Kelly, K. Kitajima, A. Strickland, J. H. Fournelle, and J. W. Valley (2013), In situ $\delta^{18}O$ and Mg/Ca analyses of diagenetic and planktic foraminiferal calcite preserved in a deep-sea record of the Paleocene-Eocene thermal maximum, *Paleoceanography*, *28*, 517–528, doi:10.1002/palo.20048.

Kroopnick, P. M. (1985), The distribution of ^{13}C of ΣCO_2 in the world oceans, *Deep Sea Res. Oceanogr. Res. Paper*, *32*(1), 57–84.

Laskar, J., P. Robutel, F. Joutel, M. Gastineau, A. Correia, and B. Levrard (2004), A long term numerical solution for the insolation quantities of the Earth, *Astron. Astrophys.*, *428*, 261–285, doi:10.1051/0004-6361:20041335.

Lawrence, J. R., J. M. Gieskes, and W. S. Broecker (1975), Oxygen isotope and cation composition of DSDP pore waters and the alteration of Layer II basalts, *Earth Planet. Sci. Lett.*, *27*, 1–10, doi:10.1016/0012-821X(75)90154-5.

Lear, C. H., H. Elderfield, and P. A. Wilson (2000), Cenozoic deep-sea temperatures and global ice volumes from Mg/Ca in benthic foraminiferal calcite, *Science*, *287*(5451), 269–272, doi:10.1126/science.287.5451.269.

Lear, C. H., E. M. Mawbey, and Y. Rosenthal (2010), Cenozoic benthic foraminiferal Mg/Ca and Li/Ca records: Toward unlocking temperatures and saturation states, *Paleoceanography*, *25*, PA4215, doi:10.1029/2009PA001880.

Ma, W. T., J. Tian, Q. Y. Li, and P. X. Wang (2011), Simulation of long eccentricity (400-kyr) cycle in ocean carbon reservoir during Miocene climate optimum: Weathering and nutrient response to orbital change, *Geophys. Res. Lett.*, *38*, L10701, doi:10.1029/2011GL047680.

Mackensen, A., H.-W. Hubberten, T. Bickert, G. Fischer, and D. K. Fütterer (1993), The $\delta^{13}C$ in benthic foraminiferal tests of *Fontbotia wuellerstorfi* (Schwager) relative to the $\delta^{13}C$ of dissolved inorganic carbon in Southern Ocean deep water: Implications for glacial ocean circulation models, *Paleoceanography*, *8*(5), 587–610, doi:10.1029/93PA01291.

McCorkle, D. C., P. A. Martin, D. W. Lea, and G. P. Klinkhammer (1995), Evidence of a dissolution effect on benthic foraminiferal shell chemistry: $\delta^{13}C$, Cd/Ca, Ba/Ca, and Sr/Ca results from the Ontong Java Plateau, *Paleoceanography*, *10*(4), 699–714, doi:10.1029/95PA01427.

McCrea, J. M. (1950), On the isotopic chemistry of carbonates and a paleotemperature scale, *J. Chem. Phys.*, *18*(6), 849–857, doi:10.1063/1.1747785.

Miller, K. G., J. D. Wright, and R. G. Fairbanks (1991), Unlocking the ice house: Oligocene–Miocene oxygen isotopes, eustasy, and margin erosion, *J. Geophys. Res.*, *96*(B4), 6829–6848, doi:10.1029/90JB02015.

Mook, W. G. (1986), ^{13}C in atmospheric CO_2, *Neth. J. Sea Res.*, *20*(2/3), 211–223.

Ohneiser, C., G. Acton, J. E. T. Channell, G. S. Wilson, Y. Yamamoto, and T. Yamazaki (2013), A middle Miocene relative paleointensity record from the equatorial Pacific, *Earth Planet. Sci. Lett.*, *374*, 227–238, doi:10.1016/j.epsl.2013.04.038.

O'Neil, J. R., R. N. Clayton, and T. K. Mayeda (1969), Oxygen isotope fractionation in divalent metal carbonates, *J. Chem. Phys.*, *51*(12), 5547–5558, doi:10.1063/1.1671982.

Paillard, D., L. Labeyrie, and P. Yiou (1996), Macintosh program performs time-series analysis, *Eos Trans. AGU*, *77*(39), 379, doi:10.1029/96EO00259.

Pälike, H., R. D. Norris, J. O. Herrle, P. A. Wilson, H. K. Coxall, C. H. Lear, N. J. Shackleton, A. K. Tripati, and B. S. Wade (2006), The heartbeat of the Oligocene climate system, *Science*, *314*(5807), 1894–1898, doi:10.1126/science.1133822.

Pälike, H., M. Lyle, H. Nishi, I. Raffi, K. Gamage, A. Klaus, and the Expedition 320/321 Scientists (2010), Proc. IODP, 320/321: Tokyo, Integrated Ocean Drilling Program Management International, Inc.

Pälike, H., et al. (2012), A Cenozoic record of the equatorial Pacific carbonate compensation depth, *Nature*, *488*(7413), 609–614, doi:10.1038/nature11360.

Pearson, P. N., and C. E. Burgess (2008), Foraminifer test preservation and diagenesis: Comparison of high latitude Eocene sites, *Geol. Soc. Lond. Spec. Publ.*, *303*, 59–72, doi:10.1144/SP303.5.

Pearson, P. N., P. W. Ditchfield, J. Singano, K. G. Harcourt-Brown, C. J. Nicholas, R. K. Olsson, N. J. Shackleton, and M. A. Hall (2001), Warm tropical sea surface temperatures in the Late Cretaceous and Eocene epochs, *Nature*, *413*(6855), 481–487, doi:10.1038/35097000.

Pearson, P. N., B. E. van Dongen, C. J. Nicholas, R. D. Pancost, S. Schouten, J. M. Singano, and B. S. Wade (2007), Stable warm tropical climate through the Eocene epoch, *Geology*, *35*, 211–214, doi:10.1130/G23175A.1.

Pearson, P. N., S. L. Evans, and J. Evans (2015), Effect of diagenetic recrystallization on the strength of planktonic foraminifer tests und compression, *J. Micropalaeontol.*, *34*(1), 59–64, doi:10.1144/jmpaleo2013-032.

Regenberg, M., D. Nürnberg, J. Schönfeld, and G.-J. Reichart (2007), Early diagenetic overprint in Caribbean sediment cores and its effect on the geochemical composition of planktonic foraminifera, *Biogeosciences*, *4*, 957–973, doi:10.5194/bg-4-957-2007.

Richter, F. M. (1993), Fluid flow in deep-sea carbonate: Estimates based on pore water Sr, *Earth Planet. Sci. Lett.*, *119*(1–2), 133–141, doi:10.1016/0012-821X(93)90011-W.

Schrag, D. P. (1999), Effects of diagenesis on the isotopic record of late Paleogene tropical sea surface temperatures, *Chem. Geol.*, *161*(1–3), 215–224, doi:10.1016/S0009-2541(99)00088-1.

Schrag, D. P., D. J. DePaolo, and F. M. Richter (1995), Reconstructing past sea surface temperatures: Correcting for diagenesis of bulk marine carbonate, *Geochim. Cosmochim. Acta*, *59*, 2265–2278, doi:10.1016/0016-7037(95)00105-9.

Sexton, P. F., and P. A. Wilson (2009), Preservation of benthic foraminifera and reliability of deep-sea temperature records: Importance of sedimentation rates, lithology, and the need to examine test wall structure, *Paleoceanography*, *24*, PA2208, doi:10.1029/2008PA001650.

Sexton, P. F., P. A. Wilson, and P. N. Pearson (2006), Microstructural and geochemical perspectives on planktic foraminiferal preservation: "Glassy" versus "Frosty", *Geochem. Geophys. Geosyst.*, *7*, Q12P19, doi:10.1029/2006GC001291.

Shackleton, N. J., and J. P. Kennett (1975), Paleotemperature history of the Cenozoic and the initiation of Antarctic glaciation: Oxygen and carbon analyses in DSDP Sites 277, 279, and 281, in *Init. Repts. DSDP 29*, edited by J. P. Kennett et al., *Deep Sea Drilling Project*, pp. 743–755, U.S. Gov. Print. Off., Washington, D. C., doi:10.2973/dsdp.proc.29.117.1975.

Shevenell, A. E., J. P. Kennett, and D. W. Lea (2004), Middle Miocene Southern Ocean cooling and Antarctic cryosphere expansion, *Science*, *305*, 1766–1770, doi:10.1126/science.1100061.

Shevenell, A. E., J. P. Kennett, and D. W. Lea (2008), Middle Miocene ice sheet dynamics, deep-sea temperatures, and carbon cycling: A Southern Ocean perspective, *Geochem. Geophys. Geosyst.*, *9*, Q02006, doi:10.1029/2007GC001736.

Stewart, D. R. M., P. N. Pearson, P. W. Ditchfield, and J. M. Singano (2004), Miocene tropical Indian Ocean temperatures: evidence from three exceptionally preserved foraminiferal assemblages from Tanzania, *J. Afr. Earth Sci.*, *40*, 173–190, doi:10.1016/j.jafrearsci.2004.09.001.

Stout, P. M. (1985), Interstitial water chemistry and diagenesis of biogenic sediments from the eastern equatorial Pacific, Deep Sea Drilling Project Leg-85, in *Init. Repts. DSDP 85*, edited by L. Mayer et al., pp. 805–820, U.S. Gov. Print. Off., Washington, D. C.

Tian, J., M. Yang, M. W. Lyle, R. Wilkens, and J. K. Shackford (2013), Obliquity and long eccentricity pacing of the Middle Miocene climate transition, *Geochem. Geophys. Geosyst.*, *14*, 1740–1755, doi:10.1002/ggge.20108.

Tian, J., W. Ma, M. W. Lyle, and J. K. Shackford (2014), Synchronous mid-Miocene upper and deep oceanic $\delta^{13}C$ changes in the east equatorial Pacific linked to ocean cooling and ice sheet expansion, *Earth Planet. Sci. Lett.*, *406*, 72–80, doi:10.1016/j.epsl.2014.09.013.

Vincent, E., and W. H. Berger (1985), Carbon dioxide and polar cooling in the Miocene: The Monterey hypothesis, in *The Carbon Cycle and Atmospheric CO_2: Natural Variations Archean to Present*, vol. 32, edited by W. S. Broecker, and E. T. Sundquist, *American Geophysical Union Geophysical Monograph*, pp. 455–468, doi:10.1029/GM032p0455.

Voigt, J., E. C. Hathorne, M. Frank, H. Vollstaedt, and A. Eisenhauer (2015), Variability of carbonate diagenesis in equatorial Pacific sediments deduced from radiogenic and stable Sr isotopes, *Geochim. Cosmochim. Acta*, *148*, 360–377, doi:10.1016/j.gca.2014.10.001.

Von Herzen, R. P., R. J. Fiske, and G. H. Sutton (1971), Geothermal measurements on Leg 8, in *Init. Repts. DSDP 8*, edited by J. I. Tracey et al., Deep Sea Drilling Project, pp. 837–849, U.S. Gov. Print. Off., Washington, D. C.

Walter, L. M., T. C. W. Ku, K. Muehlenbachs, W. P. Patterson, and L. Bonnell (2007), Controls on the $\delta^{13}C$ of dissolved inorganic carbon in marine pore waters: An integrated case study of isotope exchange during syndepositional recrystallization of biogenic carbonate sediments (South Florida Platform, USA), *Deep Sea Res., Part II*, *54*, 1163–1200, doi:10.1016/j.dsr2.2007.04.014.

Wilkens, R. H., G. R. Dickens, J. Tian, J. Backman, and the Expedition 320/321 Scientists (2013), Revised composite depth scales for Sites U1336, U1337, and U1338, in *Proc. IODP, 320/321: Tokyo*, edited by H. Pälike et al., Integrated Ocean Drilling Program Management International, Inc., doi:10.2204/iodp.proc.320321.209.2013.

Woodruff, F., and S. Savin (1991), Mid-Miocene isotope stratigraphy in the deep sea: High resolution correlations, paleoclimatic cycles, and sediment preservation, *Paleoceanography*, *6*, 755–806, doi:10.1029/91PA02561.

Zachos, J., M. Pagani, L. Sloan, E. Thomas, and K. Billups (2001b), Trends, rhythms, and aberrations in global climate 65 Ma to present, *Science*, *292*(5517), 686–693, doi:10.1126/science.1059412.

Zachos, J. C., N. J. Shackleton, J. S. Revenaugh, H. Palike, and B. P. Flower (2001a), Climate response to orbital forcing across the Oligocene–Miocene boundary, *Science*, *292*(5515), 274–278, doi:10.1126/science.1058288.

Zachos, J. C., G. R. Dickens, and R. E. Zeebe (2008), An early Cenozoic perspective on greenhouse warming and carbon-cycle dynamics, *Nature*, *451*(7176), 279–283, doi:10.1038/nature06588.

Zachos, J. C., H. McCarren, B. Murphy, U. Röhl, and T. Westerhold (2010), Tempo and scale of late Paleocene and early Eocene carbon isotope cycles: Implications for the origin of hyperthermals, *Earth Planet. Sci. Lett.*, *299*(1–2), 242–249, doi:10.1016/j.epsl.2010.09.004.

Zeebe, R. E. (1999), An explanation of the effect of seawater carbonate concentration on foraminiferal oxygen isotopes, *Geochim. Cosmochim. Acta*, *63*(13–14), 2001–2007, doi:10.1016/S0016-7037(99)00091-5.

Zeebe, R. E., J. Bijima, and D. A. Wolf-Gladrow (1999), A diffusion-reaction model of carbon isotope fractionation in foraminifera, *Mar. Chem.*, *64*(3), 199–227, doi:10.1016/S0304-4203(98)00075-9.